Journal of Wasit for Science and Medicine 2026: 19, (3), 1-10

Numerical Model of MHD Influence on Casson Blood Flow in Bifurcated Stenosed Artery

Esam Abdul Alameer Ahmed Alnussairy

Department of Biology, College of Science, Wasit University, Wasit, Iraq.

Abstract

This study computationally examines the magnetohydrodynamic (MHD) influence on blood flow dynamics in a bifurcated artery with mild stenosis. An external transverse magnetic field was used to study the complicated changes in blood flow under a constant Reynolds number (Re = 300) and a certain level of blockage (δ = 0.51375). The mathematical model assesses critical physiological characteristics, such as dimensionless pressure drop, wall shear stress, and flow streamline topologies, under different magnetic intensities (M = 0, 4, and 8). The results show that there is a direct positive relationship between the magnetic parameter and the pressure decrease across the stenosis, parent artery, and daughter artery. Also, using the magnetic field makes the wall shear much stronger, making both positive and negative peak fluctuations near the geometric limits worse. Streamline visualizations are very important because they show that in the purely hydrodynamic situation (M = 0), there are clear flow separations and recirculation eddies downstream of the stenosis. However, adding the magnetic field stops these secondary flows. The Lorentz force that is created helps keep things stable by reducing the number of disturbed recirculation zones. To validate the suggested model, the current numerical results were compared with existing literature, revealing substantial concordance. In the end, these results show that external magnetic fields can organize and stabilize complex disturbed flow fields, even though they increase flow resistance and local shear stress. This has important implications for bio-magnetic therapy and the study of how cardiovascular disease progresses.

Keywords: Numerical simulation, MAC method, bifurcated stenosed artery, pressure correction, and Casson fluid.

1. Introduction

Cardiovascular diseases remain the most common cause of morbidity and death worldwide, and most of these disorders are caused by Atherosclerosis. This disorder leads

to accumulation of plaque such as fatty substances, cholesterol, and cellular waste on the walls of arteries, making them narrower, and this process is called stenosis. Estimating blood flow in straight arteries is relatively easy, whereas blood flow in branching networks is more complex.

The bifurcations, which are the points where one vessel divides into two branch vessels, are very important anatomical structures plaque are likely to develop due to flow separation, secondary flows, and areas of low Wall Shear Stress (WSS) [1]. Stenosis near the bifurcation point leads to the generation of jet-like velocities, recirculation zones, and turbulence that can accelerate disease progression [2]. Studying these dynamics requires the use of complex mathematical models that go beyond the basic fluid mechanics. Magnetohydrodynamics (MHD) is concerned with studying how external magnetic fields affect the flow of blood, an electrically conductive fluid made up of ions and hemoglobin. The interaction of the fluid with the magnetic field generates a Lorentz force, which changes the shape of the velocity and can be used to create MRI safer and target drugs with magnets [3].

Bakheet and his colleagues have made significant contributions to the mathematical modeling of MHD blood flow in stenosed geometries. Through their research, extremely important insights were gained into the behavior of non-Newtonian blood models in the presence of magnetic fields. For example, Bakheet et al. (2018) developed a generalized power-law model to consider MHD blood flow with heat transfer, which aids to understand how blood behaves when exposed to magnetic fields [4]. In addition, their study of MHD micropolar blood flow demonstrated how magnetic fields affect blood flow through multiple stenosed arteries [5]. Their subsequent research on the Casson fluid model revealed that magnetic fields can greatly reduce wall shear stress and mitigate flow instability in regions of extreme constriction [6].

Based on these basic investigations, recent studies have focused on the intricate geometry of bifurcations. To extend these concepts to include bifurcated arteries, the effect of heat sources on MHD flow through stenosed bifurcations and elucidating is investigated and the effect of magnetic factors on temperature distribution at the flow divider is clarified [3, 7]. Zain and Ismail (2023) showed that magnetic fields might stabilize irregular flow and mitigate flow reversal in overlapping stenosis sites [8]. Similarly, computational research by Kumar et al. (2021) and Dubey et al. (2021) has incorporated non-Newtonian models, like Carreau-Yasuda, into bifurcation analysis, confirming that the interaction of MHD and bifurcation geometry establishes distinct stress patterns that differ from those found in straight vessels [9-10]. In Iqbal et al. (2024) , fluid-structure interaction

(FSI) was recently used to illustrate these magnetic forces affect the kinetics of plaque formation in bifurcated regions [11].

Although the current literature has contributed to the understanding of MHD bio-fluid dynamics, a significant gap still exists. Previous researchers have successfully identified the flow resistance and pressure reduction in individual narrowed arteries across a variety of physical situations. including [8, 11], and [12], recent studies on bifurcation geometries have mostly focused on temperature distributions, velocity profiles, and WSS.

However, there is a notable lack of comprehensive research on the distribution of hemodynamic pressure specifically within a bifurcated artery influenced by MHD. Blood pressure is one of the important physiological measurements. Excessive pressure drop across a bifurcation point can lead to hypo perfusion (insufficient blood flow) in tissues downstream, while excessive pressure gradient may cause plaque rupture. Most current bifurcation models do not adequately define how the Lorentz force interacts with the complex secondary flows at the bifurcation point to influence the pressure gradient. For the safety of patients with cardiovascular implants or who are receiving magnetic therapies, it is important to know whether the magnetic field improves the pressure drop caused by the stenosis.

Therefore, the main objective of this research is to study the distinctive effect of MHD on blood pressure and the reduction of pressure across a stenosed bifurcation artery. This study seeks to build a mathematical model and numerically solve the governing equations to create a comprehensive map of pressure variations, leading to new insights into the use of magnetic fields to modulate hemodynamic pressure within complex artery networks.

2. Governing Equations

The blood streaming is considered as a Casson fluid with two dimensions in the cylindrical polar coordinate system. The governing equations of blood motion can be written in conservative form as:

$$\frac{1}{r}\frac{\partial}{\partial r}(ru)+\frac{\partial}{\partial x}(w)=0 \tag{1}$$

$$\begin{aligned}&\frac{\partial w}{\partial t}+\frac{\partial(wu)}{\partial r}+\frac{\partial w^{2}}{\partial x}+\frac{wu}{r}\\&=-\frac{1}{\rho}\frac{\partial \mathrm{P}}{\partial x}-\frac{1}{\mathrm{Re}}\left[\frac{1}{r}\frac{\partial(r\tau_{rx})}{\partial r}+\frac{\partial(\tau_{xx})}{\partial x}+M^{2}w\right]\end{aligned} \tag{2}$$

$$\begin{aligned}&\frac{\partial u}{\partial t}+\frac{\partial u^{2}}{\partial r}+\frac{\partial(uw)}{\partial x}+\frac{u^{2}}{r}\\&=-\frac{1}{\rho}\frac{\partial \mathrm{P}}{\partial r}-\frac{1}{\mathrm{Re}}\left[\frac{1}{r}\frac{\partial(r\tau_{rr})}{\partial r}+\frac{\partial(\tau_{rz})}{\partial x}\right]\end{aligned} \tag{3}$$

where the radial and axial dimensionless r and x are scaled with respect to $R_{0.}$ The dimensionless axial and radial components w and u are scaled with respect to the cross-sectional average velocity U_0, Reynolds number Re, the dimensionless pressure $P,$ the dimensionless shear stress

τ_{ij} and the Hartmann number M can be defined respectively, as:

$$\mathrm{Re}=\frac{\rho U_0 R_0}{\eta},\ \mathrm{P}=\frac{\mathrm{P}'}{\rho U_0^2},\ \tau_{ij}=\frac{\tau'_{ij}R_0}{\eta U_0},\ \text{and}\ M=R_0B_0\sqrt{\frac{\sigma}{\mu}}$$

here B_0 is the external magnetic field and σ is the electrical conductivity. Whereas the rheological of Casson model fluid is assumed by Fung [13].

$$\tau_{xx}=-2\mu(J_2)\left(\frac{\partial w}{\partial x}\right), \quad (4)$$

$$\tau_{rr}=-2\mu(J_2)\left(\frac{\partial u}{\partial r}\right), \quad (5)$$

$$\tau_{rx}=-\mu(J_2)\left(\frac{\partial w}{\partial r}+\frac{\partial u}{\partial x}\right), \quad (6)$$

$$\text{with}\quad \mu(J_2)=\left[2^{-0.5}\tau_y{}^{0.5}+J_2{}^{0.25}\right]^2 J_2{}^{0.5}, \quad (7)$$

$$\text{where}\quad J_2=\left[2\left\{\left(\frac{\partial w}{\partial x}\right)^2+\left(\frac{\partial u}{\partial r}\right)^2+\left(\frac{u}{r}\right)^2\right\}+\left(\frac{\partial w}{\partial r}+\frac{\partial u}{\partial x}\right)^2\right],$$

(8)

Now, the condition of Casson flow is set as:

$$e_{ij}=\begin{cases}0 & \text{if}\quad J_2{}^*<\tau_y^2\\ \dfrac{1}{2\mu(J_2)}\tau_{ij} & \text{if}\quad J_2{}^*\geq\tau_y^2\end{cases}$$

where $J_2^*=0.5\tau_{ij}\tau_{ij}$ is the stress tensor in the second invariant.

Here,

$\mu(J_2)$, $J_2=0.5e_{ij}e_{ij}$, τ_y and η represent the apparent viscosity, the strain tensor invariant rate, the yield stress and coefficient of viscosity, respectively. The geometric model of this work is a portion of a bifurcated artery exhibiting mild stenosis following [12, 13, 7, 18]. The functions $R_1(x)$ and $R_2(x)$, which represent the inner and outer walls of the artery, respectively (Figure 1), are given by:

$$R_1(x)=\begin{cases}1 & ;\ 0\leq x\leq d;\ d+L_0\leq x\leq x_1\\ 1-\dfrac{4\delta}{L_0^2}\left\{(x-d)L_0-(x-d)^2\right\} & ;\ d\leq x\leq d+L_0\\ 1+r_1-\sqrt{r_1^2-(x-x_1)^2} & ;\ x_1\leq x<x_2\\ 2r_1'\sec\phi+(x-x_2)\tan\phi & ;\ x_2\leq x\leq x_{\max}\end{cases}$$

(9)

$$R_2(x)=\begin{cases}0, & 0\leq x<x_3\\ \sqrt{r_2^2-(x-x_3-r_2)^2}, & x_3\leq x<x_3+r_2(1-sin\phi)\\ r_2cos\phi+x_4, & x_3+r_2(1-sin\phi)\leq x\leq x_{\max}\end{cases}$$

(10)

Were

$$r_1=\frac{(1-2r_1'\sec\phi)}{(\cos\phi-1)};\ r_2=\frac{(x_3-x_2)\sin\phi}{1-\sin\phi};$$

$$x_2=x_1+(1-2r_1'\sec\phi)\frac{\sin\phi}{\cos\phi-1};$$

$$x_3=x_2+0.5\,;\ x_4=(x-(x_3+r_2(1-\sin\phi)))\tan\phi$$

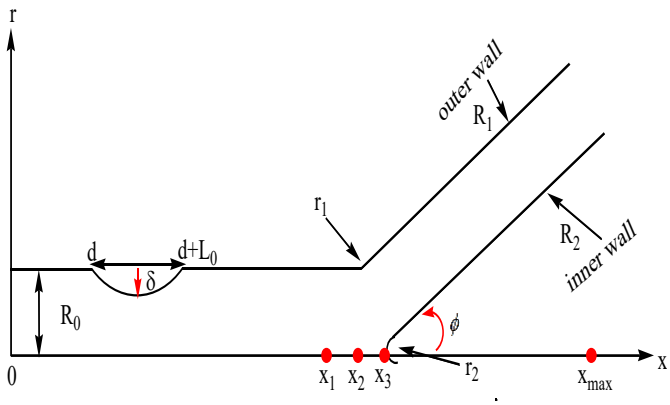

Figure1: Geometry of bifurcated stenosed artery model.

2.1 Boundary Conditions

It assumed that there is no-slip condition, meaning the blood flow velocity components are zero at the wall. The inlet velocity conditions for the Casson fluid may be taken as [13].

$$\begin{cases} w(r,0,t)=\left[\left(1-\left(\frac{r}{R}\right)^2\right)-\frac{8}{3}\sqrt{\frac{r_c}{R}}\left(1-\sqrt{\frac{r^3}{R^3}}\right)+2\frac{r_c}{R}\left(1-\frac{r}{R}\right)\right]U_0(t) \text{ if } r_c \le r \le R(x), \\ w(r,0,t)=\left[(1-\frac{8}{3}\sqrt{\frac{r_c}{R}}+2\frac{r_c}{R}-\frac{1}{3}\left(\frac{r}{R}\right)^2)\right]U_0(t) \quad \text{if} \quad 0\le r\le r_c, \\ \text{and } u(r,0,t)=0, \end{cases}$$

(11)

the radius of the plug flow is denoted by r_c , and for inlet velocity we have:

$$U_o(t)=\begin{cases} 1, & \text{for steady velocity} \\ 1-\varepsilon_{u_z}\left[1+\cos(\omega t+\delta_o\right], & \text{for pulsatile velocity,} \end{cases}$$

with $U_o(0)=0$ where the angular frequency is ω, having the similar stroke volume as the physiological stream. Using the condition $U_o(0)=0$, then $\delta_O=\cos^{-1}\left\{\frac{(1-\varepsilon_{u_z})}{\varepsilon_{u_z}}\right\}$.

The outlet velocities conditions are:

$$\frac{\partial w(r,x,t)}{\partial x}=0=\frac{\partial u(r,x,t)}{\partial x} \text{ at } x=x_{\max}$$

The problem's boundary and initial conditions are established as follows:

$$w(r,x,t)=0=u(r,x,t) \text{ on } r=R_1(x)$$
$$\text{and } r=R_2(x), x_3\le x\le x_{\max}$$

(12)

$$\frac{\partial w(r,x,t)}{\partial r}=0 \text{ on } r=0,\ 0\le \mathrm{x}\le \mathrm{x}_3$$

(13)

$$w(r,x,t)=u(r,x,t)=p(r,x,0)=0, \text{ for } x>0$$

(14)

2.2 Radical Transformation

The radical transformation is presented:

$$\xi=\frac{r-R_2(x)}{R(x)}, R(x)\neq 0,$$

(15)

where the wall of the artery is immobilized in the transformed coordinate by $R_1(x)$ and $R_2(x)$. Using Equation (15), then Equations (1)–(3) take the form:

$$(\xi R+R_2)\frac{\partial w}{\partial x}-\frac{\xi R+R_2}{R}\left(\xi\frac{\partial R}{\partial x}+\frac{\partial R_2}{\partial x}\right)\frac{\partial w}{\partial \xi}+\frac{\partial(u(\xi R+R_2)/R)}{\partial \xi}=0$$

(16)

$$\frac{\partial w}{\partial t}=-\frac{\partial p}{\partial x}+\frac{1}{R}\left(\xi\frac{\partial R}{\partial x}+\frac{\partial R_2}{\partial x}\right)\frac{\partial p}{\partial \xi}+\mathrm{Con}w+\frac{1}{\mathrm{Re}}\mathrm{Diff}w$$

(17)

$$\frac{\partial u}{\partial t}=-\frac{1}{R}\frac{\partial p}{\partial \xi}+\mathrm{Con}u+\frac{1}{\mathrm{Re}}\mathrm{Diff}u$$

(18)

where

$$\mathrm{Con}w=-\frac{1}{R}\frac{\partial(uw)}{\partial \xi}-\frac{uw}{\xi R+R_2}-\frac{\partial w^2}{\partial x}+\frac{1}{R}\left(\xi\frac{\partial R}{\partial x}+\frac{\partial R_2}{\partial x}\right)\frac{\partial w^2}{\partial \xi}$$

(19)

$$\mathrm{Diff}w=\frac{\partial^2 w}{\partial x^2}-\frac{2}{R}\left(\xi\frac{\partial R}{\partial x}+\frac{\partial R_2}{\partial x}\right)\frac{\partial^2 w}{\partial x\,\xi}+\frac{1}{R^2}\left(1+\left(\xi\frac{\partial R}{\partial x}+\frac{\partial R_2}{\partial x}\right)^2\right)\frac{\partial^2 w}{\partial \xi^2}+$$
$$\frac{1}{R}\left(\frac{1}{\xi R+R_2}\frac{\partial \tau_{\zeta x}}{\partial \zeta}+\frac{\tau_{xx}}{\zeta R}+\frac{2}{R}\frac{\partial R}{\partial x}\left(\xi\frac{\partial R}{\partial x}+\frac{\partial R_2}{\partial x}\right)-\frac{\partial \tau_{xx}}{\partial \zeta}\left(\xi\frac{\partial^2 R}{\partial x^2}+\frac{\partial^2 R_2}{\partial x^2}\right)\right)\frac{\partial w}{\partial \xi}+M^2 w$$

(20)

$$\mathrm{Con}u=-\frac{1}{R}\frac{\partial u^2}{\partial \xi}-\frac{u^2}{\xi R+R_2}-\frac{\partial(wu)}{\partial x}+\frac{1}{R}\left(\xi\frac{\partial R}{\partial x}+\frac{\partial R_2}{\partial x}\right)\frac{\partial(wu)}{\partial \xi}$$

(21)

$$\mathrm{Diff}u=\frac{\partial^2 u}{\partial x^2}-\frac{2}{R}\left(\xi\frac{\partial R}{\partial x}+\frac{\partial R_2}{\partial x}\right)\frac{\partial^2 u}{\partial x\,\xi}+\frac{1}{R^2}\left(1+\left(\xi\frac{\partial R}{\partial x}+\frac{\partial R_2}{\partial x}\right)^2\right)\frac{\partial^2 u}{\partial \xi^2}+$$
$$\frac{1}{R}\left(\frac{1}{\xi R+R_2}\frac{\partial \tau_{\zeta\zeta}}{\partial \zeta}+\frac{\tau_{\zeta\zeta}}{\zeta R}+\frac{\partial \tau_{\zeta\zeta}}{\partial x}+\frac{2}{R}\frac{\partial R}{\partial x}\left(\xi\frac{\partial R}{\partial x}+\frac{\partial R_2}{\partial x}\right)-\frac{\partial \tau_{\zeta\zeta}}{\partial \zeta}\left(\xi\frac{\partial^2 R}{\partial x^2}+\frac{\partial^2 R_2}{\partial x^2}\right)\right)\frac{\partial u}{\partial \xi}-\frac{u}{(\xi R+R_2)^2}$$

(22)

Similarly, equation (15) is utilized to

transform the conditions (12)-(14) with $\xi \in [0,1]$.

$$w(\xi,x,t) = U_{\max}\left(1-\xi^2\right), u(\xi,x,t) = 0 \text{ for } x = 0 \quad (23)$$

$$w(\xi,x,t) = 0 = u(\xi,x,t) \text{ on } \xi = R_1(x) \text{ and } \xi = R_2(x), x_3 \le x \le x_{\max} \quad (24)$$

$$\frac{\partial w(\zeta,x,t)}{\partial \zeta} = 0 \text{ on } \zeta = 0,\ 0 \le \mathrm{x} \le \mathrm{x}_3 \quad (25)$$

$$w(\zeta,x,t) = u(\zeta,x,t) = p(\zeta,x,0) = 0, \text{ for } x > 0 \quad (26)$$

The Marker and Cell (MAC) method is used to discretize the unsteady governing equations (16) through (18). Then we calculated the pressure and velocities at different points. Defining $\zeta = j\Delta\zeta,\ x = i\Delta x,\ t = n\Delta t$ and $p(\zeta,x,t) = p(j\Delta\zeta, i\Delta x, n\Delta t) = p_{i,j}^n$, where t is the time, Δt is the increment of t, and $\Delta x, \Delta\zeta$ are represented the length and width of the control volume cell (i, j) respectively.

2. 3 Governing Equations Discretization

At the (i, j) th cell, the governing equations are discretized yield:

$$(\xi_{lj}R_{li}^n + R_{2li}^n)\left(\frac{w_{i,j}^n - w_{i-1,j}^n}{\Delta x}\right) - \frac{\xi_{lj}R_{li}^n + R_{2li}^n}{R_{li}^n}\left(\xi_{lj}\left(\frac{\partial R}{\partial x}\right)_{li}^n + \left(\frac{\partial R_2}{\partial x}\right)_{li}^n\right)\left(\frac{w_{at} - w_{ab}}{\Delta\xi}\right) + \frac{(\xi_j R_i^n + R_{2i}^n)u_{i,j}^n - (\xi_{j-1}R_i^n + R_{2i}^n)u_{i,j-1}^n}{R_i^n \Delta\xi} = 0 \quad (27)$$

where

$$w_{at} = \frac{w_{i,j}^n + w_{i-1,j}^n + w_{i-1,j+1}^n + w_{i,j+1}^n}{4} \quad (28)$$

$$w_{ab} = \frac{w_{i,j}^n + w_{i-1,j}^n + w_{i-1,j-1}^n + w_{i-1,j-1}^n}{4} \quad (29)$$

$$\zeta_{lj} = \zeta_j - \frac{\Delta\zeta}{2},\ R^n = R(x_{lj}),\ x_{lj} = x_i - \frac{\Delta x}{2}$$

and

$$\frac{w_{i,j}^{n+1} - w_{i,j}^n}{\Delta t} = \left(\frac{p_{i,j}^n - p_{i+1,j}^n}{\Delta x}\right) + \frac{1}{R_i^n}\left(\xi_{lj}\left(\frac{\partial R}{\partial x}\right)_i^n + \left(\frac{\partial R_2}{\partial x}\right)_i^n\right)\left(\frac{p_t - p_b}{\Delta\xi}\right) + wcd_{i,j}^n \quad (30)$$

where $wcd_{i,j}^n = \mathrm{Con}w_{i,j}^n + \frac{1}{\mathrm{Re}}\left(\mathrm{Diff}w_{i,j}^n\right)$ (31)

$$\frac{u_{i,j}^{n+1} - u_{i,j}^n}{\Delta t} = -\frac{1}{R_{lj}^n}\left(\frac{p_{i,j}^n - p_{i,j+1}^n}{\Delta\xi}\right) + ucd_{i,j}^n \quad (32)$$

Where $ucd_{i,j}^n = \mathrm{Con}u_{i,j}^n + \frac{1}{\mathrm{Re}}\left(\mathrm{Diff}u_{i,j}^n\right)$ (33)

with $\mathrm{Con}u_{i,j}^n$ and $\mathrm{Diff}u_{i,j}^n$ are the convective and diffusive terms and they are differences in the same manner to the *w*- equation of momentum. The complete numerical procedure and stability restriction have already enclosed in [5].

3. Results and Discussion

Validating numbers, the study compares results to those of Alnussairy *et al.* (2025) [12]. Figure 2 shows the outcome of the dimensionless axial velocity profile of a Casson model that was made using the MAC approach, which is at the point of maximum constriction. The model observed that the baseline Newtonian case (τ = 0) perfectly aligns with [12]. As the yield stress parameter

(τ) increases from 0 to 1, the velocity increases at the center of the artery.

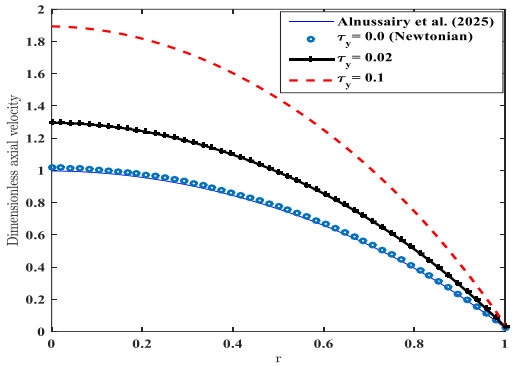

Figure 2: Validation of dimensionless axial velocity with [12].

Table 1. Diminsinless pressure drop cross the artery at different magnetic intensities.

M	0	8
Pressure cross stenosis	4.1936	7.5238
Pressure crosses in the main parent	11.4638	16.5923
Pressure crosses in the daughter artery	21.4025	44.3101

Table 1 shows how the magnetic parameter (M) affects the dimensionless pressure drop across three different parts of a bifurcated artery: the stenosis, the main parent artery, and the daughter artery. The data shows that the pressure drop across all measured portions is directly related to the strength of the magnetic field. As the magnetic parameter goes from 0 (no magnetic field) to 8, the pressure drop across the stenosis goes from 4.1936 to 7.5238, and in the major parent artery, it goes from 11.4638 to 16.5923. The daughter's artery is where the pressure drop has the biggest effect. The magnetic field makes the pressure drop more than double, going from 21.4025 to 44.3101.

Physically, the Lorentz force is what causes this event to happen. When an external magnetic field is introduced to a fluid that conducts electricity, like blood, it creates a resistive force that opposes against the flow of the blood. This magnetic pull slows down the blood flow, which makes it harder for the blood to circulate. Because of this, a much larger pressure gradient is needed to keep the flow rate through the narrower stenosis and branching sections. This is why the table shows such a large increase in pressure drops.

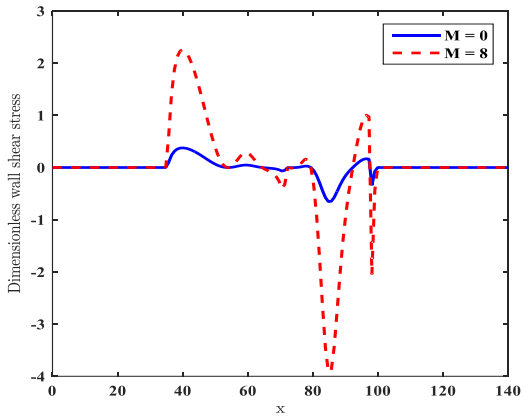

Figure. 3: Dimensionless WSS with for M =0 and for M =8.

Figure 3 shows how the dimensionless wall shear stress changes along the axial distance (x) for both the hydrodynamic case (M = 0) and the magnetohydrodynamic case (M = 8). The graph shows that using a magnetic field greatly increases the size of the

wall shear stress changes. At the first big change (about $x = 40$), the positive wall shear stress goes up a lot when the magnetic field is present. For $M = 8$, it peaks at about 2.2, while for $M = 0$, it peaks at about 0.4. There is a clear area of negative wall shear stress further downstream, between $x = 80$ and $x = 100$. The magnetic field makes this negative peak much stronger, dropping it to around -4.0 for $M = 8$. In the non-magnetic case ($M = 0$), the dip is much shallower, about -0.6.

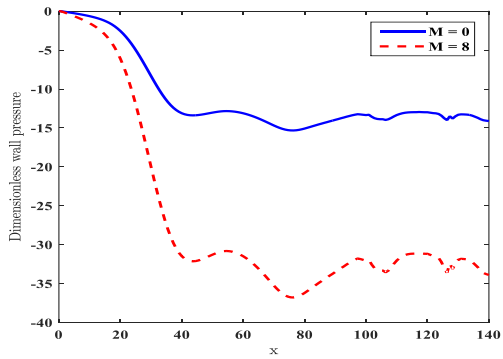

Figure 4: Variation of wall pressure for M with along axial x position.

Figure 4 demonstrates the variation of dimensionless wall pressure along the artery for M=0 and M=8. Both profiles start at the inlet x=0 with zero value and experience a substantial drop into negative values as the blood flows downstream. The presentation of the magnetic field significantly increases the magnitude of the pressure drop. For M=0, the wall pressure decreases and oscillates slightly around -15. In contrast, when the pressure drop is greatly steeper and more severe, approximately oscillating between -30 and -37 downstream. This shows that an increase in M significantly enhances the flow resistance, causing a higher pressure to drop along the artery.

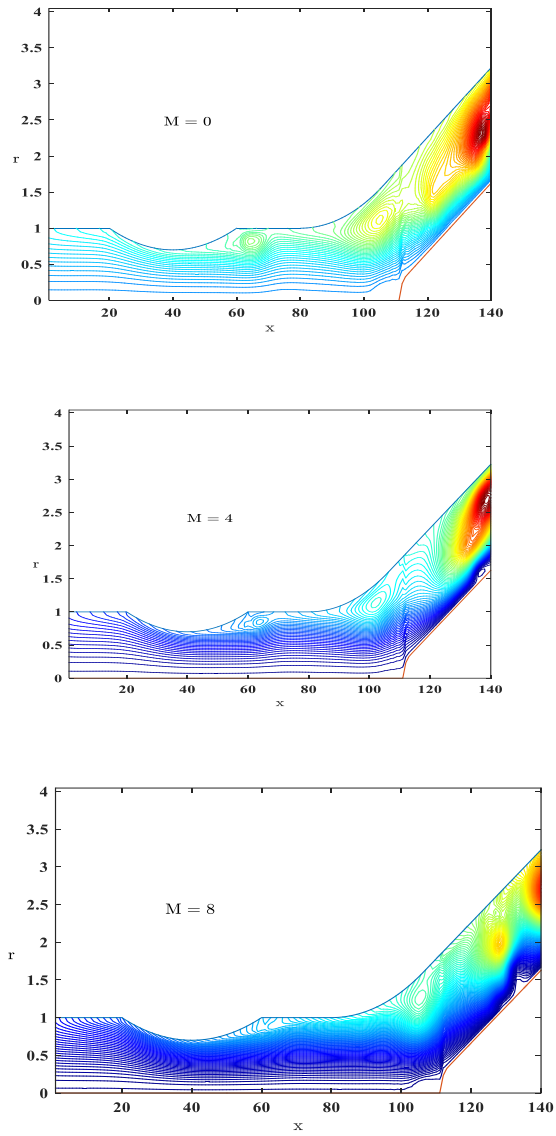

Figure 5: Streamline of blood flow patterns in parent and daughter artery for varying M.

Figure 5 presents the streamline contours of blood flow in the parent and daughter arteries under varying magnetic intensities (M = 0, 4, and 8), maintaining a constant Reynolds number (Re = 300) and an occlusion parameter (δ = 0.51375). In the non-magnetic case (M = 0), prominent

recirculation zones (vortices or eddies) are clearly visible downstream of the stenosis and near the outer wall of the bifurcation. As the magnetic parameter is introduced and increased to M = 4 and subsequently to M = 8, these secondary recirculation zones are progressively suppressed. At the highest magnetic intensity (M = 8), the flow separation is heavily minimized, and the streamlines become significantly smoother and more aligned with the geometry of the arterial walls. As a result, the magnetic field stabilizes the blood, making it easier for it to overcome the adverse pressure gradient and making the overall flow more organized and streamlined through the complicated geometry.

4. Conclusion

This research computationally investigated MHD effects on blood flow in a bifurcated artery presenting mild stenosis. W can come to several important conclusions. Increase in Pressure Drop: A transverse magnetic field greatly increases flow resistance. As a result, the dimensionless pressure drops across all parts of the artery, including the stenosis, the primary parent artery, and the daughter artery, increases a lot as M increases. The branching daughter artery has the most dramatic variations in pressure gradient. Amplification of WSS, where the external magnetic field significantly modifies the distribution of shear stress along the artery walls. Because of the magnetic field (M = 8), the velocity gradients near the boundary get steeper. This causes very large positive and negative peak fluctuations in wall shear stress, especially in areas where the geometry changes, such the stenosis throat and bifurcation areas. Preventing Flow Separation: Streamline visualizations show that when there is no magnetic field (M = 0), the post-stenotic and bifurcation areas are quite likely to have flow separation and recirculation eddies. When a strong magnetic field is added, though, it creates a resistive Lorentz force that effectively dampens these changes in speed. When the magnetic parameter goes up to M = 4 and M = 8, the secondary recirculation zones get smaller, which makes the flow pattern more stable and structured.

5. References

1. Shahzadi I., and Bilal S., (2020). A significant role of permeability on blood flow for hybrid nanofluid through bifurcated stenosed artery: Drug delivery application. Computer Methods and Programs in Biomedicine. 187, 105248.
2. Chakravarty S., and Mandal P. K., (2000). Two-dimensional blood flow through tapered arteries under stenotic conditions. International Journal of Non-Linear Mechanics. 35, 779–793.
3. Prakash J., Ogulu A., and Makinde O. D., (2011). A study of effects of heat source

on MHD blood flow through bifurcated arteries. AIP Advances. 1, 042128.

4. Bakheet A., Alnussairy E. A., Ismail Z., and Amin N., (2018). Generalized power-law model of magnetohydrodynamic blood flow with heat transfer. Indian Journal of Public Health Research and Development. 9, 794.
5. Alnussairy E. A., and Bakheet A., (2019). MHD micropolar blood flow model through a multiple stenosed artery. AIP Conference Proceedings. 2183, 100003.
6. Bakheet A., and Alnussairy E. A., (2021). Numerical Simulation of Magnetohydrodynamic Influences on Casson Model for Blood Flow through an Overlapping Stenosed Artery. Iraqi Journal of Science. 62, 1016–1024.
7. Rao K. V., Reddy P. R., and Rao M. V., (2021). Mathematical modeling of blood flow through a stenosed bifurcated artery with heat source and magnetic effect. Communications in Mathematics and Applications. 12, 1005-1011.
8. Zain F. M., and Ismail Z., (2023). Numerical solution of magnetohydrodynamics effects on a generalised power law fluid model of blood flow through a bifurcated artery with an overlapping shaped stenosis. PLOS ONE. 18, e0276576.
9. Kumar D., Satyanarayana B., Kumar R., Kumar S., and Deo N., (2021). Application of heat source and chemical reaction in MHD blood flow through permeable bifurcated arteries with inclined magnetic field in tumor treatments. Results in Applied Mathematics. 10, 100151.
10. Dubey A., Vasu B., Bég O. A., and Gorla R. S. R., (2021). Finite element computation of magneto-hemodynamic flow and heat transfer in a bifurcated artery with saccular aneurysm using non-Newtonian Casson model. Microvascular Research. 138, 104221.
11. Iqbal K., Rossi di Schio E., Anwar M. A., Razzaq M., Shahzad H., Valdiserri, P., and Biserni C., (2024). A Fluid–Structure Interaction Analysis to Investigate the Influence of Magnetic Fields on Plaque Growth in Stenotic Bifurcated Arteries. Dynamics. 4, 3, 572-591.
12. Alnussairy A., Noman L. M., and Bakheet A., (2025). Predicting Hemodynamic Alterations Due to Bifurcation Stenosis: A Mathematical Model and Numerical Analysis of Newtonian Blood Flow. Mathematical Modelling and Engineering Problems. 12, 4122-4128.
13. Fung Y. C., (1981). Biomechanics: Mechanical Properties of Living Tissues. Springer, Berlin.
14. Bakheet A., Alnussairy E. A., Ismail Z., and Amin N., (2016). Blood flow through an inclined stenosed artery. Applied Mathematical Sciences, 10, 235-254.